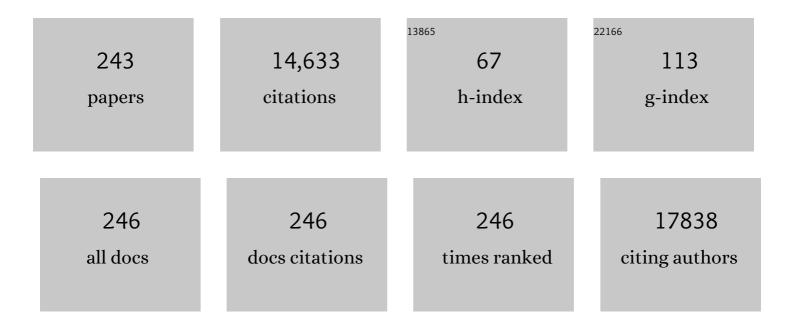
List of Publications by Year in descending order

Source: https://exaly.com/author-pdf/7179488/publications.pdf Version: 2024-02-01



#	Article	IF	CITATIONS
1	Understanding Heterogeneities in Quantum Materials. Advanced Materials, 2023, 35, e2106909.	21.0	8
2	Selective Antisite Defect Formation in WS <sub>2</sub> Monolayers via Reactive Growth on Dilute Wâ€Au Alloy Substrates. Advanced Materials, 2022, 34, e2106674.	21.0	14
3	Mesoscale interplay between phonons and crystal electric field excitations in quantum spin liquid candidate CsYbSe <sub>2</sub> . Journal of Materials Chemistry C, 2022, 10, 4148-4156.	5.5	5
4	Photoluminescence Induced by Substitutional Nitrogen in Single-Layer Tungsten Disulfide. ACS Nano, 2022, 16, 7428-7437.	14.6	7
5	Stabilized Synthesis of 2D Verbeekite: Monoclinic PdSe <sub>2</sub> Crystals with High Mobility and In-Plane Optical and Electrical Anisotropy. ACS Nano, 2022, 16, 13900-13910.	14.6	14
6	Heterogeneities at multiple length scales in 2D layered materials: From localized defects and dopants to mesoscopic heterostructures. Nano Research, 2021, 14, 1625-1649.	10.4	8
7	Waveform analysis of a large-area superconducting nanowire single photon detector. Superconductor Science and Technology, 2021, 34, 035020.	3.5	4
8	Intrinsic Defects in MoS <sub>2</sub> Grown by Pulsed Laser Deposition: From Monolayers to Bilayers. ACS Nano, 2021, 15, 2858-2868.	14.6	40
9	Strain-Induced Growth of Twisted Bilayers during the Coalescence of Monolayer MoS <sub>2</sub> Crystals. ACS Nano, 2021, 15, 4504-4517.	14.6	19
10	Understanding Substrate-Guided Assembly in van der Waals Epitaxy by <i>in Situ</i> Laser Crystallization within a Transmission Electron Microscope. ACS Nano, 2021, 15, 8638-8652.	14.6	7
11	Signature of Many-Body Localization of Phonons in Strongly Disordered Superlattices. Nano Letters, 2021, 21, 7419-7425.	9.1	1
12	Excitonic Dynamics in Janus MoSSe and WSSe Monolayers. Nano Letters, 2021, 21, 931-937.	9.1	86
13	Nonâ€Equilibrium Synthesis of Highly Active Nanostructured, Oxygenâ€Incorporated Amorphous Molybdenum Sulfide HER Electrocatalyst. Small, 2020, 16, e2004047.	10.0	29
14	Permanently Magnetized Insulating Thinâ€Film Devices by Reduction. Physica Status Solidi - Rapid Research Letters, 2020, 14, 2000346.	2.4	0
15	Enhancement of van der Waals Interlayer Coupling through Polar Janus MoSSe. Journal of the American Chemical Society, 2020, 142, 17499-17507.	13.7	80
16	Giant enhancement of exciton diffusivity in two-dimensional semiconductors. Science Advances, 2020, 6, .	10.3	12
17	Twoâ€Ðimensional Palladium Diselenide with Strong Inâ€₽lane Optical Anisotropy and High Mobility Grown by Chemical Vapor Deposition. Advanced Materials, 2020, 32, e1906238.	21.0	81
18	Low Energy Implantation into Transition-Metal Dichalcogenide Monolayers to Form Janus Structures. ACS Nano, 2020, 14, 3896-3906.	14.6	136

#	Article	IF	CITATIONS
19	Anisotropic Phonon Response of Fewâ€Layer PdSe <sub>2</sub> under Uniaxial Strain. Advanced Functional Materials, 2020, 30, 2003215.	14.9	26
20	Atomically Precise PdSe2 Pentagonal Nanoribbons. ACS Nano, 2020, 14, 1951-1957.	14.6	21
21	In situ laser reflectivity to monitor and control the nucleation and growth of atomically thin 2D materials*. 2D Materials, 2020, 7, 025048.	4.4	14
22	Engineering Edge States of Graphene Nanoribbons for Narrow-Band Photoluminescence. ACS Nano, 2020, 14, 5090-5098.	14.6	27
23	In Quest of a Ferromagnetic Insulator: Structure-Controlled Magnetism in Mg–Ti–O Thin Films. Journal of Physical Chemistry C, 2019, 123, 19970-19978.	3.1	8
24	Size, structure, and luminescence of Nd2Zr2O7 nanoparticles by molten salt synthesis. Journal of Materials Science, 2019, 54, 12411-12423.	3.7	19
25	Room-Temperature Electron–Hole Liquid in Monolayer MoS <sub>2</sub> . ACS Nano, 2019, 13, 10351-10358.	14.6	49
26	lsotope-Engineering the Thermal Conductivity of Two-Dimensional MoS <sub>2</sub> . ACS Nano, 2019, 13, 2481-2489.	14.6	42
27	Strain tolerance of two-dimensional crystal growth on curved surfaces. Science Advances, 2019, 5, eaav4028.	10.3	46
28	Atomic Insight into Thermolysisâ€Ðriven Growth of 2D MoS <sub>2</sub> . Advanced Functional Materials, 2019, 29, 1902149.	14.9	28
29	Defect-Mediated Phase Transformation in Anisotropic Two-Dimensional PdSe <sub>2</sub> Crystals for Seamless Electrical Contacts. Journal of the American Chemical Society, 2019, 141, 8928-8936.	13.7	81
30	Samarium-Activated La <sub>2</sub> Hf <sub>2</sub> O <sub>7</sub> Nanoparticles as Multifunctional Phosphors. ACS Omega, 2019, 4, 17956-17966.	3.5	44
31	Roomâ€Temperature Insulating Ferromagnetic (Ni,Co) 1+2 x Ti 1â^' x O 3 Thin Films. Annalen Der Physik, 2019, 531, 1900299.	2.4	7
32	Structure determination of oxamic acid from laboratory powder X-Ray diffraction data and energy minimization by DFT-D. Journal of Molecular Structure, 2019, 1177, 310-316.	3.6	2
33	Realâ€Time Observation of Orderâ€Disorder Transformation of Organic Cations Induced Phase Transition and Anomalous Photoluminescence in Hybrid Perovskites. Advanced Materials, 2018, 30, e1705801.	21.0	60
34	Anomalous interlayer vibrations in strongly coupled layered PdSe <sub>2</sub> . 2D Materials, 2018, 5, 035016.	4.4	60
35	Exploring Anomalous Polarization Dynamics in Organometallic Halide Perovskites. Advanced Materials, 2018, 30, 1705298.	21.0	44
36	Phonon localization in heat conduction. Science Advances, 2018, 4, eaat9460.	10.3	108

#	Article	IF	CITATIONS
37	Ultrafast Exciton Dissociation at the 2D-WS <sub>2</sub> Monolayer/Perovskite Interface. Journal of Physical Chemistry C, 2018, 122, 28910-28917.	3.1	23
38	Organohalide Perovskites: Real-Time Observation of Order-Disorder Transformation of Organic Cations Induced Phase Transition and Anomalous Photoluminescence in Hybrid Perovskites (Adv.) Tj ETQq0 0 0 r	gBI1¦Over	loak 10 Tf 50
39	Persistent Photomagnetism in Superparamagnetic Iron Oxide Nanoparticles. Advanced Electronic Materials, 2018, 4, 1700661.	5.1	5
40	Two-channel model for ultralow thermal conductivity of crystalline Tl <sub>3</sub> VSe <sub>4</sub> . Science, 2018, 360, 1455-1458.	12.6	206
41	Ultrafast Spectral Dynamics of CsPb(Br <sub><i>x</i></sub> Cl <sub>1–<i>x</i></sub> ) <sub>3</sub> Mixed-Halide Nanocrystals. ACS Photonics, 2018, 5, 3575-3583.	6.6	44
42	Photocarrier Transfer across Monolayer MoS <sub>2</sub> –MoSe <sub>2</sub> Lateral Heterojunctions. ACS Nano, 2018, 12, 7086-7092.	14.6	25
43	Anatomy of a Visible Light Activated Photocatalyst for Water Splitting. ACS Catalysis, 2018, 8, 6650-6658.	11.2	24
44	DNA Methylation Detection Using Resonance andÂNanobowtie-Antenna-Enhanced Raman Spectroscopy. Biophysical Journal, 2018, 114, 2498-2506.	0.5	21

46	Complex and Noncentrosymmetric Stacking of Layered Metal Dichalcogenide Materials Created by Screw Dislocations. Journal of the American Chemical Society, 2017, 139, 3496-3504.	13.7	81
47	Black Anatase Formation by Annealing of Amorphous Nanoparticles and the Role of the Ti <sub>2</sub> O <sub>3</sub> Shell in Self-Organized Crystallization by Particle Attachment. ACS Applied Materials & Interfaces, 2017, 9, 22018-22025.	8.0	15
48	Edge-Controlled Growth and Etching of Two-Dimensional GaSe Monolayers. Journal of the American Chemical Society, 2017, 139, 482-491.	13.7	65

Oxidization stability of atomically precise graphene nanoribbons. Physical Review Materials, 2018, 2, .

49	Nanostructured carbon electrocatalyst supports for intermediate-temperature fuel cells: Single-walled versus multi-walled structures. Journal of Power Sources, 2017, 337, 145-151.	7.8	12
50	Interlayer bond polarizability model for stacking-dependent low-frequency Raman scattering in layered materials. Nanoscale, 2017, 9, 15340-15355.	5.6	38
51	Synthesis and Photoluminescence Properties of 2D Phenethylammonium Lead Bromide Perovskite Nanocrystals. Small Methods, 2017, 1, 1700245.	8.6	27
52	PdSe <sub>2</sub> : Pentagonal Two-Dimensional Layers with High Air Stability for Electronics. Journal of the American Chemical Society, 2017, 139, 14090-14097.	13.7	509
53	Seamless Staircase Electrical Contact to Semiconducting Graphene Nanoribbons. Nano Letters, 2017, 17, 6241-6247.	9.1	64
54	Bottom up synthesis of boron-doped graphene for stable intermediate temperature fuel cell	10.3	23

electrodes. Carbon, 2017, 123, 605-615.

#	Article	IF	CITATIONS
55	Nonequilibrium Synthesis of TiO <sub>2</sub> Nanoparticle "Building Blocks―for Crystal Growth by Sequential Attachment in Pulsed Laser Deposition. Nano Letters, 2017, 17, 4624-4633.	9.1	33
56	Suppression of Defects and Deep Levels Using Isoelectronic Tungsten Substitution in Monolayer MoSe <sub>2</sub> . Advanced Functional Materials, 2017, 27, 1603850.	14.9	84
57	High-temperature magnetostructural transition in van der Waals-layered <mml:math xmlns:mml="http://www.w3.org/1998/Math/MathML"&gt; <mml:mrow> <mml:mi>α </mml:mi> <mml:mtext>â^ Physical Review Materials, 2017, 1, .</mml:mtext></mml:mrow></mml:math 	:natext> <r< td=""><td>ท<b>ธฬ</b>:msub&gt;&lt;</td></r<>	ท <b>ธฬ</b> :msub><
58	In-Plane Heterojunctions Enable Multiphasic Two-Dimensional (2D) MoS <sub>2</sub> Nanosheets As Efficient Photocatalysts for Hydrogen Evolution from Water Reduction. ACS Catalysis, 2016, 6, 6723-6729.	11.2	116
59	Raman Study of the Structural Distortion in the Ni <sub>1–<i>x</i></sub> Co <sub><i>x</i></sub> TiO <sub>3</sub> Solid Solution. Inorganic Chemistry, 2016, 55, 9436-9444.	4.0	24
60	Persistent photoconductivity in two-dimensional Mo <sub>1â^'<i>x</i></sub> W <sub><i>x</i></sub> Se <sub>2</sub> –MoSe <sub>2</sub> van der Waals heterojunctions. Journal of Materials Research, 2016, 31, 923-930.	2.6	20
61	In-Plane Optical Anisotropy of Layered Gallium Telluride. ACS Nano, 2016, 10, 8964-8972.	14.6	179
62	Ultrafast Dynamics of Metal Plasmons Induced by 2D Semiconductor Excitons in Hybrid Nanostructure Arrays. ACS Photonics, 2016, 3, 2389-2395.	6.6	42
63	Isoelectronic Tungsten Doping in Monolayer MoSe <sub>2</sub> for Carrier Type Modulation. Advanced Materials, 2016, 28, 8240-8247.	21.0	85
64	Tailoring Vacancies Far Beyond Intrinsic Levels Changes the Carrier Type and Optical Response in Monolayer MoSe <sub>2â^'<i>x</i></sub> Crystals. Nano Letters, 2016, 16, 5213-5220.	9.1	121
65	Two-dimensional GaSe/MoSe <sub>2</sub> misfit bilayer heterojunctions by van der Waals epitaxy. Science Advances, 2016, 2, e1501882.	10.3	239
66	Ultrafast Charge Transfer and Hybrid Exciton Formation in 2D/0D Heterostructures. Journal of the American Chemical Society, 2016, 138, 14713-14719.	13.7	102
67	Interlayer Coupling in Twisted WSe <sub>2</sub> /WS <sub>2</sub> Bilayer Heterostructures Revealed by Optical Spectroscopy. ACS Nano, 2016, 10, 6612-6622.	14.6	249
68	Nanoscale Silicon as a Catalyst for Graphene Growth: Mechanistic Insight from <i>in Situ</i> Raman Spectroscopy. Journal of Physical Chemistry C, 2016, 120, 14180-14186.	3.1	10
69	Low-Frequency Interlayer Raman Modes to Probe Interface of Twisted Bilayer MoS <sub>2</sub> . Nano Letters, 2016, 16, 1435-1444.	9.1	177
70	Twisted MoSe <sub>2</sub> Bilayers with Variable Local Stacking and Interlayer Coupling Revealed by Low-Frequency Raman Spectroscopy. ACS Nano, 2016, 10, 2736-2744.	14.6	117
71	Carbon Nanotubes Grown on Metal Microelectrodes for the Detection of Dopamine. Analytical Chemistry, 2016, 88, 645-652.	6.5	113
72	Improving Light Harvesting in Dye-Sensitized Solar Cells Using Hybrid Bimetallic Nanostructures. ACS Photonics, 2016, 3, 385-394.	6.6	64

#	Article	IF	CITATIONS
73	Thickness-dependent charge transport in few-layer MoS <sub>2</sub> field-effect transistors. Nanotechnology, 2016, 27, 165203.	2.6	124
74	Anisotropic Electron-Photon and Electron-Phonon Interactions in Black Phosphorus. Nano Letters, 2016, 16, 2260-2267.	9.1	328
75	Ultrathin nanosheets of CrSiTe <sub>3</sub> : a semiconducting two-dimensional ferromagnetic material. Journal of Materials Chemistry C, 2016, 4, 315-322.	5.5	235
76	Observation of two distinct negative trions in tungsten disulfide monolayers. Physical Review B, 2015, 92, .	3.2	44
77	Controllable Growth of Perovskite Films by Roomâ€īemperature Air Exposure for Efficient Planar Heterojunction Photovoltaic Cells. Angewandte Chemie - International Edition, 2015, 54, 14862-14865.	13.8	41
78	Revealing the Preferred Interlayer Orientations and Stackings of Twoâ€Đimensional Bilayer Gallium Selenide Crystals. Angewandte Chemie, 2015, 127, 2750-2755.	2.0	5
79	Revealing the Preferred Interlayer Orientations and Stackings of Twoâ€Dimensional Bilayer Gallium Selenide Crystals. Angewandte Chemie - International Edition, 2015, 54, 2712-2717.	13.8	45
80	Phase transitions and thermal-stress-induced structural changes in a ferroelectric Pb(Zr <sub>0.80</sub> Ti <sub>0.20</sub> )O <sub>3</sub> single crystal. Journal of Physics Condensed Matter, 2015, 27, 025901.	1.8	5
81	Van der Waals Epitaxial Growth of Two-Dimensional Single-Crystalline GaSe Domains on Graphene. ACS Nano, 2015, 9, 8078-8088.	14.6	103
82	Patterned arrays of lateral heterojunctions within monolayer two-dimensional semiconductors. Nature Communications, 2015, 6, 7749.	12.8	213
83	Perovskite Solar Cells with Near 100% Internal Quantum Efficiency Based on Large Single Crystalline Grains and Vertical Bulk Heterojunctions. Journal of the American Chemical Society, 2015, 137, 9210-9213.	13.7	246
84	Low-Frequency Raman Fingerprints of Two-Dimensional Metal Dichalcogenide Layer Stacking Configurations. ACS Nano, 2015, 9, 6333-6342.	14.6	151
85	Low-Frequency Interlayer Breathing Modes in Few-Layer Black Phosphorus. Nano Letters, 2015, 15, 4080-4088.	9.1	182
86	Structure and Formation Mechanism of Black TiO <sub>2</sub> Nanoparticles. ACS Nano, 2015, 9, 10482-10488.	14.6	170
87	Nonlinear Fano-Resonant Dielectric Metasurfaces. Nano Letters, 2015, 15, 7388-7393.	9.1	474
88	Equally Efficient Interlayer Exciton Relaxation and Improved Absorption in Epitaxial and Nonepitaxial MoS <sub>2</sub> /WS <sub>2</sub> Heterostructures. Nano Letters, 2015, 15, 486-491.	9.1	337
89	Interaction of carbon nanohorns with plants: Uptake and biological effects. Carbon, 2015, 81, 607-619.	10.3	196
90	Exploring growth kinetics of carbon nanotube arrays by in situ optical diagnostics and modeling. Proceedings of SPIE, 2014, , .	0.8	0

#	Article	IF	CITATIONS
91	Catalytic nanoparticles for carbon nanotube growth synthesized by through thin film femtosecond laser ablation. Proceedings of SPIE, 2014, , .	0.8	1
92	Slowing of femtosecond laser-generated nanoparticles in a background gas. Applied Physics Letters, 2014, 105, 213108.	3.3	6
93	Cooperative Island Growth of Large-Area Single-Crystal Graphene on Copper Using Chemical Vapor Deposition. ACS Nano, 2014, 8, 5657-5669.	14.6	91
94	Pulsed Laser Deposition of Photoresponsive Twoâ€Ðimensional GaSe Nanosheet Networks. Advanced Functional Materials, 2014, 24, 6365-6371.	14.9	108
95	Digital Transfer Growth of Patterned 2D Metal Chalcogenides by Confined Nanoparticle Evaporation. ACS Nano, 2014, 8, 11567-11575.	14.6	47
96	Nanoparticle generation and transport resulting from femtosecond laser ablation of ultrathin metal films: Time-resolved measurements and molecular dynamics simulations. Applied Physics Letters, 2014, 104, .	3.3	42
97	Revealing the surface and bulk regimes of isothermal graphene nucleation and growth on Ni with in situ kinetic measurements and modeling. Carbon, 2014, 79, 256-264.	10.3	16
98	Controlled Vapor Phase Growth of Single Crystalline, Two-Dimensional GaSe Crystals with High Photoresponse. Scientific Reports, 2014, 4, 5497.	3.3	222
99	Real-time optical diagnostics of graphene growth induced by pulsed chemical vapor deposition. Nanoscale, 2013, 5, 6507.	5.6	22
100	Nature of the band gap and origin of the electro-/photo-activity of Co3O4. Journal of Materials Chemistry C, 2013, 1, 4628.	5.5	176
101	Fluorination of "brick and mortar―soft-templated graphitic ordered mesoporous carbons for high power lithium-ion battery. Journal of Materials Chemistry A, 2013, 1, 9414.	10.3	23
102	High-temperature transformation of Fe-decorated single-wall carbon nanohorns to nanooysters: a combined experimental and theoretical study. Nanoscale, 2013, 5, 1849-1857.	5.6	10
103	A statistical model approximation for perovskite solid-solutions: A Raman study of lead-zirconate-titanate single crystal. Journal of Applied Physics, 2013, 113, .	2.5	32
104	Nature of Catalytic Active Sites Present on the Surface of Advanced Bulk Tantalum Mixed Oxide Photocatalysts. ACS Catalysis, 2013, 3, 2920-2929.	11.2	56
105	Uniform, Homogenous Coatings of Carbon Nanohorns on Arbitrary Substrates from Common Solvents. ACS Applied Materials & Interfaces, 2013, 5, 13153-13160.	8.0	23
106	Fundamental Bulk/Surface Structure–Photoactivity Relationships of Supported (Rh2–yCryO3)/GaN Photocatalysts. Journal of Physical Chemistry Letters, 2013, 4, 3719-3724.	4.6	32
107	Spatial and temporal measurements of temperature and cell viability in response to nanoparticle-mediated photothermal therapy. Nanomedicine, 2012, 7, 1729-1742.	3.3	14
108	Near-field enhanced ultraviolet resonance Raman spectroscopy using aluminum bow-tie nano-antenna. Applied Physics Letters, 2012, 101, 113116.	3.3	46

#	Article	IF	CITATIONS
109	Metal-assisted hydrogen storage on Pt-decorated single-walled carbon nanohorns. Carbon, 2012, 50, 4953-4964.	10.3	69
110	Incremental Growth of Short SWNT Arrays by Pulsed Chemical Vapor Deposition. Small, 2012, 8, 1534-1542.	10.0	9
111	Flux-Dependent Growth Kinetics and Diameter Selectivity in Single-Wall Carbon Nanotube Arrays. ACS Nano, 2011, 5, 8311-8321. Vibrational spectrum of the endohedral <mml:math< td=""><td>14.6</td><td>33</td></mml:math<>	14.6	33
112	xmlns:mml="http://www.w3.org/1998/Math/MathML" display="inline"> <mml:mrow><mml:msub><mml:mi mathvariant="normal"&gt;Y<mml:mrow><mml:mn>2</mml:mn></mml:mrow></mml:mi </mml:msub>xmlns:mml="http://www.w3.org/1998/Math/MathML" display="inline"&gt;<mml:mrow><mml:msub><mml:mrow< td=""><td>&gt; {/mml:m 3.2</td><td>ath&gt;C<mm< td=""></mm<></td></mml:mrow<></mml:msub></mml:mrow></mml:mrow>	> {/mml:m 3.2	ath>C <mm< td=""></mm<>
113	/> <mml:mrow><mml:mn>2</mml:mn></mml:mrow> @C <mml:math Antioxidant Deactivation on Graphenic Nanocarbon Surfaces. Small, 2011, 7, 2775-2785.</mml:math 	10.0	133
114	Single walled carbon nanohorns as photothermal cancer agents. Lasers in Surgery and Medicine, 2011, 43, 43-51.	2.1	67
115	Raman study of Fano interference in <i>p</i> â€ŧype doped silicon. Journal of Raman Spectroscopy, 2010, 41, 1759-1764.	2.5	49
116	Narrow and intense resonances in the low-frequency region of surface-enhanced Raman spectra of single-wall carbon nanotubes. Physical Review B, 2010, 82, .	3.2	8
117	Separation of junction and bundle resistance in single wall carbon nanotube percolation networks by impedance spectroscopy. Applied Physics Letters, 2010, 97, .	3.3	56
118	Investigation ofGd3N@C2nâ€,(40≤≤4)family by Raman and inelastic electron tunneling spectroscopy. Physical Review B, 2010, 81, .	3.2	25
119	Pulsed Growth of Vertically Aligned Nanotube Arrays with Variable Density. ACS Nano, 2010, 4, 7573-7581.	14.6	41
120	In Vitro and in Vivo Studies of Single-Walled Carbon Nanohorns with Encapsulated Metallofullerenes and Exohedrally Functionalized Quantum Dots. Nano Letters, 2010, 10, 2843-2848.	9.1	56
121	A Facile High-speed Vibration Milling Method to Water-disperse Single-walled Carbon Nanohorns. Chemistry of Materials, 2010, 22, 347-351.	6.7	22
122	Investigation of Gd2@C90, Gd2C2@C92, and Gd2@C79N by Raman Spectroscopy. Materials Research Society Symposia Proceedings, 2009, 1204, 1.	0.1	3
123	Metastable Copperâ€Phthalocyanine Singleâ€Crystal Nanowires and Their Use in Fabricating Highâ€Performance Fieldâ€Effect Transistors. Advanced Functional Materials, 2009, 19, 3776-3780.	14.9	81
124	Model for Self-Assembly of Carbon Nanotubes from Acetylene Based on Real-Time Studies of Vertically Aligned Growth Kinetics. Journal of Physical Chemistry C, 2009, 113, 15484-15491.	3.1	59
125	Growth, Patterning, and One-Dimensional Electron -Transport Properties of Self-Assembled Ag-TCNQF4 Organic Nanowires. Chemistry of Materials, 2009, 21, 4275-4281.	6.7	48
126	Cumulative and continuous laser vaporization synthesis of single wall carbon nanotubes and nanohorns. Applied Physics A: Materials Science and Processing, 2008, 93, 849-855.	2.3	34

#	Article	IF	CITATIONS
127	Altering the catalytic activity of thin metal catalyst films forÂcontrolled growth of chemical vapor deposited vertically aligned carbon nanotube arrays. Applied Physics A: Materials Science and Processing, 2008, 93, 1005-1009.	2.3	8
128	Pulsed laser CVD investigations of single-wall carbon nanotube growth dynamics. Applied Physics A: Materials Science and Processing, 2008, 93, 987-993.	2.3	25
129	Selective Patterned Growth of Singleâ€Crystal Ag–TCNQ Nanowires for Devices by Vapor–Solid Chemical Reaction. Advanced Functional Materials, 2008, 18, 3043-3048.	14.9	57
130	Real-time imaging of vertically aligned carbon nanotube array growth kinetics. Nanotechnology, 2008, 19, 055605.	2.6	61
131	Formation studies and controlled production of carbon nanohorns using continuousin situcharacterization techniques. Nanotechnology, 2007, 18, 185604.	2.6	19
132	Simple model of the interrelation between single- and multiwall carbon nanotube growth rates for the CVD process. Physical Review B, 2007, 75, .	3.2	53
133	Single-Crystal Organic Nanowires of Copper–Tetracyanoquinodimethane: Synthesis, Patterning, Characterization, and Device Applications. Angewandte Chemie - International Edition, 2007, 46, 2650-2654.	13.8	90
134	The effect of annealing on the electrical and thermal transport properties of macroscopic bundles of long multi-wall carbon nanotubes. Physica B: Condensed Matter, 2007, 388, 326-330.	2.7	57
135	In situ timeâ€resolved measurements of carbon nanotube and nanohorn growth. Physica Status Solidi (B): Basic Research, 2007, 244, 3944-3949.	1.5	18
136	Imperfect surface order and functionalization in vertical carbon nanotube arrays probed by near edge X-ray absorption fine structure spectroscopy (NEXAFS). Physical Chemistry Chemical Physics, 2006, 8, 5038.	2.8	20
137	Fast and highly anisotropic thermal transport through vertically aligned carbon nanotube arrays. Applied Physics Letters, 2006, 89, 223110.	3.3	157
138	Near-Edge X-ray Absorption Fine Structure Spectroscopy as a Tool for Investigating Nanomaterials. Small, 2006, 2, 26-35.	10.0	152
139	Directed Integration of Tetracyanoquinodimethane-Cu Organic Nanowires into Prefabricated Device Architectures. Advanced Materials, 2006, 18, 2184-2188.	21.0	91
140	In situ electric-field-induced contrast imaging of electronic transport pathways in nanotube-polymer composites. Applied Physics Letters, 2006, 89, 013114.	3.3	12
141	In situ measurements and modeling of carbon nanotube array growth kinetics during chemical vapor deposition. Applied Physics A: Materials Science and Processing, 2005, 81, 223-240.	2.3	300
142	Structural control of vertically aligned multiwalled carbon nanotubes by radio-frequency plasmas. Applied Physics Letters, 2005, 87, 173106.	3.3	20
143	High-density vertically aligned multiwalled carbon nanotubes with tubular structures. Applied Physics Letters, 2005, 86, 253105.	3.3	38
144	Low Temperature Growth of Boron Nitride Nanotubes on Substrates. Nano Letters, 2005, 5, 2528-2532.	9.1	176

#	Article	IF	CITATIONS
145	A laser-deposition approach to compositional-spread discovery of materials on conventional sample sizes. Measurement Science and Technology, 2005, 16, 21-31.	2.6	20
146	Molecular Beam-Controlled Nucleation and Growth of Vertically Aligned Single-Wall Carbon Nanotube Arrays. Journal of Physical Chemistry B, 2005, 109, 16684-16694.	2.6	137
147	Rapid Growth of Long, Vertically Aligned Carbon Nanotubes through Efficient Catalyst Optimization Using Metal Film Gradients. Nano Letters, 2004, 4, 1939-1942.	9.1	88
148	In situ control of the catalyst efficiency in chemical vapor deposition of vertically aligned carbon nanotubes on predeposited metal catalyst films. Applied Physics Letters, 2004, 84, 1759-1761.	3.3	110
149	Nucleation of Single-Walled Carbon Nanotubes. Physical Review Letters, 2003, 90, 145501.	7.8	127
150	In situ growth rate measurements and length control during chemical vapor deposition of vertically aligned multiwall carbon nanotubes. Applied Physics Letters, 2003, 83, 1851-1853.	3.3	127
151	Integrally gated carbon nanotube field emission cathodes produced by standard microfabrication techniques. Journal of Vacuum Science & Technology an Official Journal of the American Vacuum Society B, Microelectronics Processing and Phenomena, 2003, 21, 957.	1.6	19
152	Synthesis of multifunctional single-wall carbon nanotube-amorphous diamond thin film composites. , 2003, , .		1
153	In situ optical absorption spectroscopy, incandencence, and light-scattering characterization of single-wall carbon nanotube synthesis by the laser vaporization technique. , 2003, 4977, 648.		0
154	Synthesis and characterization of single-wall carbon nanotube–amorphous diamond thin-film composites. Applied Physics Letters, 2002, 81, 2097-2099.	3.3	44
155	Investigations of single-wall carbon nanotube growth by time-restricted laser vaporization. Physical Review B, 2002, 65, .	3.2	87
156	<title>Laser synthesis of single-wall carbon nanotubes with time-resolved in-situ diagnostics</title> . , 2002, , .		0
157	<title>Laser synthesis of single-wall carbon nanotubes with time-resolved in situ diagnostics</title> . , 2002, 4762, 268.		0
158	Operation of individual integrally gated carbon nanotube field emitter cells. Applied Physics Letters, 2002, 81, 2860-2862.	3.3	24
159	Time-resolved diagnostics of single wall carbon nanotube synthesis by laser vaporization. Applied Surface Science, 2002, 197-198, 552-562.	6.1	26
160	The electrodeposition of metal at metal/carbon nanotube junctions. Chemical Physics Letters, 2002, 361, 525-529.	2.6	18
161	Condensed phase growth of single-wall carbon nanotubes from laser annealed nanoparticulates. Applied Physics Letters, 2001, 78, 3307-3309.	3.3	52
162	Time-resolved diagnostics and mechanisms of single-wall carbon nanotube synthesis by the laser vaporization technique. , 2001, , .		0

#	Article	IF	CITATIONS
163	<title>Computer modeling of the interaction of a laser-ablated plume with an ambient background gas</title> . , 2000, , .		0
164	<title>Dynamics of the vapor plumes produced by the MALDI technique</title> . , 2000, 4070, 166.		3
165	<title>Aspects of nanoparticle formation during pulsed laser ablation</title> ., 2000, , .		0
166	Characterization of thin-film amorphous semiconductors using spectroscopic ellipsometry. Thin Solid Films, 2000, 377-378, 68-73.	1.8	134
167	Dynamics of single-wall carbon nanotube synthesis by laser vaporization. Applied Physics A: Materials Science and Processing, 2000, 70, 153-160.	2.3	148
168	<title>In-situ plasma diagnostic investigations of single-wall carbon nanotube synthesis by laser&lt;br&gt;ablation of C-Ni-Co targets</title> . , 2000, , .		1
169	In situ imaging and spectroscopy of single-wall carbon nanotube synthesis by laser vaporization. Applied Physics Letters, 2000, 76, 182-184.	3.3	115
170	Theory and numerical modeling of the accelerated expansion of laser-ablated materials near a solid surface. Physical Review B, 1999, 60, 8373-8382.	3.2	37
171	Gas-phase nanoparticle formation and transport during pulsed laser deposition of Y1Ba2Cu3O7â^'d. Applied Physics Letters, 1999, 74, 3788-3790.	3.3	60
172	Imaging of Vapor Plumes Produced by Matrix Assisted Laser Desorption: A Plume Sharpening Effect. Physical Review Letters, 1999, 83, 444-447.	7.8	103
173	<title>Pulsed-laser-deposited amorphous diamond and related materials: synthesis, characterization, and field emission properties</title> . , 1999, , .		1
174	Mechanisms of Single-Wall Carbon Nanotube Growth by the Laser Vaporization Technique: In Situ Imaging and Spectroscopy. Materials Research Society Symposia Proceedings, 1999, 593, 3.	0.1	1
175	Gas-phase diagnostics and LIF-imaging of 3-hydroxypicolinic acid maldi-matrix plumes. Chemical Physics Letters, 1998, 286, 425-432.	2.6	74
176	Dynamics of plume propagation, splitting, and nanoparticle formation during pulsed-laser ablation. Applied Surface Science, 1998, 127-129, 151-158.	6.1	91
177	LIF imaging and gas-phase diagnostics of laser desorbed MALDI-matrix plumes. Applied Surface Science, 1998, 127-129, 248-254.	6.1	24
178	Time-resolved imaging of gas phase nanoparticle synthesis by laser ablation. Applied Physics Letters, 1998, 72, 2987-2989.	3.3	318
179	Photoluminescence from gas-suspended SiOx nanoparticles synthesized by laser ablation. Applied Physics Letters, 1998, 73, 438-440.	3.3	108
180	Dynamics of plume propagation and splitting during pulsed-laser ablation of Si in He and Ar. Physical Review B. 1998, 58, 1533-1543.	3.2	87

#	Article	IF	CITATIONS
181	Emission spectroscopy of a carbon plasma formed by laser ablation of graphite. II. Ablation by a CO2laser and also simultaneously by XeCl and CO2lasers. Quantum Electronics, 1998, 28, 33-37.	1.0	6
182	Structure and optical properties of amorphous diamond films prepared by ArF laser ablation as a function of carbon ion kinetic energy. Applied Physics Letters, 1998, 73, 2591-2593.	3.3	70
183	Amorphous Diamond Films Deposited by Pulsed-Laser Ablation: the Optimum Carbon-Ion Kinetic Energy and Effects of Laser Wavelength. Materials Research Society Symposia Proceedings, 1998, 526, 325.	0.1	18
184	Characterization of Pulsed-Laser Deposited Amorphous Diamond Films by Spectroscopic Ellipsometry. Materials Research Society Symposia Proceedings, 1998, 526, 349.	0.1	3
185	Time-Resolved Imaging and Photoluminescence of Gas-Suspended Nanoparticles Synthesized by Laser Ablation: Dynamics, Transport, Collection, and Ex Situ Analysis. Materials Research Society Symposia Proceedings, 1998, 526, 47.	0.1	1
186	In Situ Diagnostics of Nanomaterial Synthesis by Laser Ablation: Time-resolved Photoluminescence Spectra and Imaging of Gas-Suspended Nanoparticles Deposited for Thin Films. Materials Research Society Symposia Proceedings, 1998, 536, 359.	0.1	0
187	Emission spectroscopy of a carbon plasma formed by laser ablation of graphite. I. Ablation by XeCl laser radiation. Quantum Electronics, 1997, 27, 983-987.	1.0	4
188	Dynamics of Plume Propagation and Splitting during Pulsed-Laser Ablation. Physical Review Letters, 1997, 79, 1571-1574.	7.8	174
189	Computational modeling of physical processes during laser ablation. Materials Science and Engineering B: Solid-State Materials for Advanced Technology, 1997, 47, 70-77.	3.5	27
190	Synthesis of Novel Thin-Film Materials by Pulsed Laser Deposition. Science, 1996, 273, 898-903.	12.6	547
191	Modeling of dynamical processes in laser ablation. Applied Surface Science, 1996, 96-98, 14-23.	6.1	47
192	Laser ablation plume thermalization dynamics in background gases: combined imaging, optical absorption and emission spectroscopy, and ion probe measurements. Applied Surface Science, 1996, 96-98, 131-138.	6.1	75
193	Laser-solid interaction and dynamics of laser-ablated materials. Applied Surface Science, 1996, 96-98, 45-49.	6.1	35
194	Comparative diagnostics of ArF- and KrF-laser generated carbon plumes used for amorphous diamond-like carbon film deposition. Applied Surface Science, 1996, 96-98, 859-865.	6.1	50
195	Mechanisms affecting kinetic energies of laserâ€ablated materials. Journal of Vacuum Science and Technology A: Vacuum, Surfaces and Films, 1996, 14, 1111-1114.	2.1	31
196	Modeling of plume dynamics in laser ablation processes for thin film deposition of materials. Physics of Plasmas, 1996, 3, 2203-2209.	1.9	39
197	Laser-Solid Interaction and Dynamics of the Laser-Ablated Materials. Materials Research Society Symposia Proceedings, 1995, 388, 27.	0.1	5
198	Dynamical Modeling of Laser ablation Processes. Materials Research Society Symposia Proceedings, 1995, 388, 3.	0.1	0

#	Article	IF	CITATIONS
199	Pulsed Laser Ablation Growth and Doping of Epitaxial Compound Semiconductor Films. Materials Research Society Symposia Proceedings, 1995, 397, 107.	0.1	4
200	Effect of Ambient Gas Pressure on Pulsed Laser Ablation Plume Dynamics and Znte Film Growth. Materials Research Society Symposia Proceedings, 1995, 397, 119.	0.1	5
201	Species-resolved imaging and gated photon counting Spectroscopy of laser ablation plume dynamics During krf- and arf-laser pld of amorphous diamond films. Materials Research Society Symposia Proceedings, 1995, 397, 55.	0.1	25
202	Amorphous Diamond-Like Carbon Film Growth by KrF-and Arf-Excimer Laser Pld: Correlation with Plume Properties. Materials Research Society Symposia Proceedings, 1995, 388, 145.	0.1	9
203	Direct monitoring of laser absorption of MALDI matrices by fast piezoelectric transducer. Chemical Physics Letters, 1995, 234, 165-171.	2.6	2
204	Growth of highly doped pâ€ŧype ZnTe films by pulsed laser ablation in molecular nitrogen. Applied Physics Letters, 1995, 67, 2545-2547.	3.3	38
205	Dynamics of laser ablation plume penetration through low pressure background gases. Applied Physics Letters, 1995, 67, 197-199.	3.3	189
206	Vapor Breakdown During ablation by Nanosecond Laser Pulses. Materials Research Society Symposia Proceedings, 1995, 388, 133.	0.1	3
207	MonC4n Cluster Synthesis: Clarification. Science, 1995, 267, 440-441.	12.6	1
208	Laser-ablation-plume thermalization dynamics in background gases studied by time-resolved imaging, spectroscopic, and ion probe diagnostics. , 1995, 2403, 15.		1
209	Accelerated Expansion of Laser-Ablated Materials near a Solid Surface. Physical Review Letters, 1995, 75, 4706-4709.	7.8	60
210	Mo <sub> <i>n</i> </sub> C <sub> 4 <i>n</i> </sub> Cluster Synthesis: Clarification. Science, 1995, 267, 440-441.	12.6	0
211	Synthesis and Characterization of Molybdenum Carbide Clusters MonC4n, (n = 1 to 4). Science, 1994, 263, 68-71.	12.6	35
212	Modeling of Thermal, Electronic, Hydrodynamic, and Dynamic Deposition Processes for Pulsed-Laser Deposition of Thin Films. Materials Research Society Symposia Proceedings, 1994, 354, 675.	0.1	1
213	Multiphoton ionization/dissociation of osmium tetroxide. Journal of Chemical Physics, 1993, 98, 951-958.	3.0	2
214	Formation and Luminescence of Molybdenum Atoms After UV Multiphoton Excitation of Gas Phase Mo(CO)6. Laser Chemistry, 1992, 12, 223-229.	0.5	3
215	Comments on small superconducting clusters. Applied Physics A: Solids and Surfaces, 1992, 54, 100-102.	1.4	4
216	Gas-phase formation of clusters and ultra-fine particles in UV multiphoton excitation of metal carbonyls. Spectrochimica Acta Part A: Molecular Spectroscopy, 1990, 46, 509-516.	0.1	9

#	Article	IF	CITATIONS
217	Resonant raman scattering of vibrationally highly excited supersonic-jet-cooled SO2 molecules. Applied Physics B, Photophysics and Laser Chemistry, 1989, 49, 131-137.	1.5	0
218	IR-Luminescence of CF2Cl2 Molecules in Multiple-Photon Excitation With Co2-Laser Radiation. Laser Chemistry, 1988, 8, 123-135.	0.5	2
219	Multiphoton and Multifrequency Resonances in the IR Laser Excitation of OsO4 Molecules Cooled in a Supersonic Jet. Laser Chemistry, 1988, 8, 137-149.	0.5	2
220	Inverse Electronic Relaxation at IR Multiple-Photon Excitation of Molecules. Laser Chemistry, 1986, 6, 103-123.	0.5	2
221	IR MPD of CDF3 in Two-frequency IR Fields. Laser Chemistry, 1986, 6, 85-92.	0.5	9
222	Ir absorption spectrum of CrO2Cl2 molecules for high-lying states of the vibrational quasi-continuum. Chemical Physics, 1986, 106, 131-149.	1.9	18
223	Study of the visible emission induced by IR multipleâ€photon excitation of OsO4. Journal of Chemical Physics, 1986, 84, 2020-2034.	3.0	16
224	Highly selective and efficient multiphoton dissociation of polyatomic molecules in multiple-frequency IR-laser fields. Applied Physics B, Photophysics and Laser Chemistry, 1985, 36, 93-103.	1.5	43
225	Simple Method for Obtaining Multiple-Frequency Radiation From a Single CO2 Laser. Laser Chemistry, 1985, 5, 167-172.	0.5	1
226	CARS spectra of thermally excited SF6 molecules. Applied Physics B, Photophysics and Laser Chemistry, 1983, 31, 89-96.	1.5	6
227	Time of flight spectroscopy of particles in electronically excited state, produced via infrared laser excitation. Applied Physics Berlin, 1980, 22, 77-81.	1.4	12
228	Direct measurement of multiphoton molecular absorption of IR laser radiation by pyroelectric detector. Applied Physics Berlin, 1980, 22, 409-413.	1.4	34
229	Multiple-photon ir excitation of electronic states of OsO4 molecule. Applied Physics Berlin, 1980, 23, 391-401.	1.4	14
230	Influence of collisions and pulse intensity on multiple photon absorption in SF6. Optics Communications, 1980, 34, 81-85.	2.1	26
231	Multiple infrared photon absorption in OsO4. Applied Physics Berlin, 1979, 19, 75-79.	1.4	15
232	Investigation of multiple photon excitation of OsO4 by dissociation yield saturation. Optics Communications, 1978, 27, 79-84.	2.1	24
233	Characteristics of multiple-photon dissociation of OsO4 molecule by two frequency tunable CO2-laser pulses. Optics Communications, 1978, 25, 69-74.	2.1	44
234	Multiphoton absorption of OsO_4 under two-CO_2-laser pulse excitation. Optics Letters, 1978, 3, 103.	3.3	7

#	Article	IF	CITATIONS
235	Selective photoionization of atoms by laser radiation and its applications. Progress in Quantum Electronics, 1977, 5, 139-203.	7.0	70
236	On the optical probing of excited molecules that have undergone radiationless transitions. Chemical Physics Letters, 1977, 45, 583-585.	2.6	2
237	dissociation of the OsO4 molecule by intense IR laser pulses. Chemical Physics Letters, 1977, 45, 231-234.	2.6	33
238	Measuring photoionization cross-sections of excited atomic states. Applied Physics Berlin, 1976, 9, 335-337.	1.4	70
239	Isotope-selective dissociation of CCl4 molecule by excitation of composite vibrational bands by intense infrared field. Physics Letters, Section A: General, Atomic and Solid State Physics, 1976, 56, 183-185.	2.1	39
240	Selective dissociation of SF6 molecules in a two-frequency infrared laser field. Optics Communications, 1976, 18, 517-521.	2.1	109
241	Direct measurement of population on molecular vibrational levels excited by laser radiation. Chemical Physics Letters, 1972, 16, 252-254.	2.6	37
242	Dynamics of pulsed laser ablation for thin film growth. , 0, , .		0
243	Modeling and simulation of short-channel MOSFETs operating in deep weak inversion. , 0, , .		0